Plasmon-Coupled Resonance Energy Transfer II: Exploring the Peaks and Dips in the Electromagnetic Coupling Factor

Wendu Ding,[†] Liang-Yan Hsu,[*,‡] Charles W. Heaps,[†] and George C. Schatz[*,†]

†*Department of Chemistry, Northwestern University, 2145 Sheridan Road, Evanston, Illinois 60208-3113, United States*

‡*Institute of Atomic and Molecular Sciences, Academia Sinica, Taipei 10617, Taiwan*

E-mail: lyhsu@gate.sinica.edu.tw; g-schatz@northwestern.edu

Abstract

We study resonance energy transfer between a donor-acceptor pair located on opposite sides of a spherical silver nanoparticle and explore the dependence of energy transfer rate on nanoparticle size using a quantum electrodynamics theory we developed previously. This theory indicates that the rate is determined by the product of donor emission spectra, acceptor absorption spectra, and an electronic coupling factor (CF) that is determined by electrodynamics associated with the donor as a dipole emitter near the nanoparticle. We find that the CF spectra show peaks that are associated with localized surface plasmon (LSP) resonances, but the locations of the most significant peaks are less correlated to the size of the nanoparticle than is found for extinction spectra for the same particle. For small nanoparticles ($\lesssim 30\,\text{nm}$), where dipole plasmon excitation dominates, a quasi-static analysis leads to an analytical formula in which the CF peaks and dips involve interference between donor electric field and the scattered dipolar field of the nanoparticle. For larger nanoparticles ($60 - 210\,\text{nm}$), the CF maximizes at a wavelength near 355 nm independent of particle size that is determined by the highest multipole plasmon that contributes significantly to the extinction spectrum, with only small contributions arising from lower multipole plasmons such as the dipole plasmon. Also, for wavelengths near 325 nm where the bulk plasmon resonance of silver can be excited, surface plasmons cannot be excited, so excitation from the donor cannot be transmitted by surface plasmons to the acceptor, leading to a pronounced dip in the CF. This work provides new concepts concerning plasmon-mediated energy transfer that are quite different from conventional (Förster) theory, but which should dominate energy transfer behavior when donor and acceptor are sufficiently separated.

Introduction

Plasmonics is the study of the interaction between electromagnetic fields and collective oscillations of electrons in a material. In recent years, experimental and computational techniques

have advanced significantly in studies of different types of plasmons, such as surface plasmon plaritons, localized surface plasmons, and lattice plasmons. These advances enable potential applications and provide deep understanding in several fields including surface-enhanced Raman spectroscopy (SERS),[1–5] plasmonic lasers,[6–8] chemical and biological sensing,[4,9–14] and light energy conversion.[15–20]

One promising application of plasmonics is plasmon-coupled resonance energy transfer (PC-RET),[19,21–27] where the rate of resonance energy transfer (RET) is modified by nearby plasmonic nanostructures (such as a silver or gold nanoparticle). PC-RET is related to, *but distinct from*, conventional molecular RET, where the latter has seen extensive applications in such fields as photosynthesis,[28–31] molecular structure dynamics,[32–38] and sensing.[39–41] In the RET case, the rate of energy transfer between two molecules, a donor and an acceptor, can be estimated by Förster theory[42,43]

$$W_{\mathrm{ET}} = \frac{\Phi_D}{\tau_D} \frac{9000 \ln 10}{128 \pi^5 N_A} \frac{\kappa^2}{n_r^4 R^6} \int d\overline{\nu} \frac{\epsilon(\overline{\nu}) I(\overline{\nu})}{\overline{\nu}^4}, \tag{1}$$

where $\overline{\nu}$ is wavenumber, Φ_D is the fluorescence quantum yield of the donor, τ_D is the emission lifetime of the donor, N_A is Avogadro's number, n_r is the refractive index of the host medium, κ describes the relative orientation between the donor and the acceptor, R is the distance between the donor and the acceptor, $\epsilon(\overline{\nu})$ is the molar absorption coefficient of the acceptor, and $I(\overline{\nu})$ is the normalized emission spectrum of the donor. Two key concepts can be extracted from Eq. 1. The first is that the rate of RET is inversely proportional to the sixth power of the intermolecular distance (the R^{-6} term), enabling RET to function as a molecular ruler.[33,44,45] The second is the proportionality between the rate and the spectral overlap $J = \int d\overline{\nu}\ \overline{\nu}^{-4} \epsilon(\overline{\nu}) I(\overline{\nu})$, which describes the energy overlap between the donor's emission and the acceptor's absorption, and serves as a simple qualitative tool to estimate the energy transfer rate between two molecules.

Förster theory has been extensively used to determine the RET rate, but it cannot be

applied to PC-RET because of two limiting assumptions. (1) Förster theory can be applied only when the donor-acceptor pair is surrounded by a homogeneous, non-absorbing, and non-dispersive host medium. This requires that the host medium must have a frequency independent, spatially invariant, real-valued, positive dielectric constant (i.e. n_r in Eq. 1, the square root of dielectric constant, is a real, positive, constant number). If a metal nanoparticle is in the vicinity of the donor-acceptor pair, then Eq. 1 should not be used to determine the RET rate between the two molecules. (2) The assumption of electrostatic interaction between donor and acceptor implies that the intermolecular distance has to be much smaller than the excitation wavelength, which typically falls in the visible light range (i.e. $R \ll \lambda$, and R is less than 10 nm).

Previous studies show that energy transfer can be enhanced by nearby metal nanoparticles,[9,46,47] indicating the demand for a theory of energy transfer over large distances ($R >$ 10 nm). Different theoretical approaches have been explored to overcome these limitations. For example, by using quantum electrodynamics, one can extend Förster theory to include intermediate and far zone effects.[48–50] Furthermore, Dung et. al. overcame the restrictions on the host medium by expressing the RET transition amplitude in terms of dyadic Green's functions.[51] Still, determining the Green's function for an arbitrary environment is non-trivial.

A recently developed method[25,26] connects the transition amplitude to the total electric field at the location of the acceptor through

$$M(\overline{\nu}, \mathbf{r_D}, \mathbf{r_A}) = -\mu^{\mathrm{D}}\mu^{\mathrm{A}} \frac{\mathbf{e}^{\mathrm{A}} \cdot \mathbf{E}^{\mathrm{D}}(\mathbf{r_A}, \overline{\nu})}{\mathrm{p_{ex}}(\overline{\nu})}, \tag{2}$$

where $\mu^{D/A}$ stands for the transition dipole moment of the donor/acceptor (regular for magnitude, bold for vector), $\mathbf{e}^{\mathrm{A}}$ is the directional unit vector of $\boldsymbol{\mu}^{\mathrm{A}}$ (i.e. $\mathbf{e}^{\mathrm{A}} = \boldsymbol{\mu}^{\mathrm{A}}/\mu^{A}$), $\mathbf{E}^{\mathrm{D}}$ is the electric field at the position of the acceptor generated by the donor, and p_{ex} is the amplitude of dipole used to calculate $\mathbf{E}^{\mathrm{D}}$. The vector field $\mathbf{E}^{\mathrm{D}}$ can be calculated in its fully

retarded form, including the response of the surrounding environment. Eq. 2 can be expressed in terms of dyadic Green's functions.[25,26] The advantage of Eq. 2 is that one can easily evaluate M for RET for a wide range of complex dielectric environments, and with various numerical computational approaches, instead of directly solving for the complicated dyadic Greens function. It also provides a clear physical picture indicating that the transition amplitude is effectively the interaction energy between the acceptor dipole moment and the electric field generated by the donor. Incorporating Eq. 2 into Fermi's Golden Rule provides a more general expression for the rate of RET:

$$W_{\mathrm{ET}} = \frac{\phi_D}{\tau_D} \frac{9000 \ln 10}{128\pi^5 N_A} \int d\overline{\nu} \frac{\epsilon(\overline{\nu}) I(\overline{\nu})}{\overline{\nu}^4} F(\overline{\nu}) \tag{3}$$

$$F(\overline{\nu}) \equiv \left| \frac{\mathbf{e}^{\mathrm{A}} \cdot \mathbf{E}^{\mathrm{D}}(\mathbf{r_A}, \overline{\nu})}{\mathrm{p_{ex}}(\overline{\nu})} \right|^2 \tag{4}$$

which is applicable for energy transfer processes in any inhomogeneous, absorbing, and dispersive medium, provided that the magnetic permeabilities of all materials in the system are 1. The variable $F(\overline{\nu})$ is the coupling factor (CF) of a donor-acceptor pair. The main difference between Eq. 3 and Eq. 1 is the inclusion of the effects of orientation, distance, and host medium response in the generalized spectral overlap (GSO),[26] which is the overlap of the donor emission spectrum, acceptor absorption spectrum, and the CF spectrum. In Förster theory, the rate of energy transfer is proportional to the spectral overlap. Similarly, in PC-RET, the rate is proportional to GSO. Furthermore, the modification to the RET rate described by the CF depends on frequency due to the frequency-dependent plasmonic behavior of the nearby nanoparticles. Therefore, in order to understand and utilize PC-RET, it is necessary to understand the physical nature of the CF in the frequency domain.

In this work, the coupling factor, F, is examined as a function of both nanoparticle size and the dipole emission wavelength. Using Mie theory for the electrodynamics calculations, we analyze the peaks and dips in the CF spectra for a donor-acceptor pair separated by a silver nanoparticle when varying the nanoparticle size. The origins of dips and peaks

in the CF spectra are explained by comparing to quasi-static approximation results and decomposing the vector spherical harmonics solutions from Mie theory. In the end, we conclude that the CF is mainly influenced by the two factors: the nanoparticle-size dependent multipole resonances (localized surface plasmons, or LSPs) and the characteristics of the silver dielectric function. In addition, the wavelength dependence of the CF is quite different from that of the extinction or scattering spectra for the same nanoparticle, with the CF optical response dominated by the highest multipole plasmon that can be excited, while extinction is dominated by low order LSPs.

Theory

Electrodynamics calculation

The calculation of the PC-RET transition amplitude requires the electric field associated with donor emission that is evaluated at the location of the acceptor. In this work, an extension of Mie theory is used to calculate the electrodynamic response of the nanoparticle due to emission by the donor, where the donor is treated as an oscillating point dipole source.[52–56] The incident field and scattered field can be expressed using the basis of vector spherical harmonics (VSH):

$$\mathbf{E}_{\text{inc}} = \sum_{l=1}^{\infty} \sum_{m=-l}^{l} [p_{lm} \mathbf{N}_{lm}^{(1)}(k\mathbf{r}) + q_{lm} \mathbf{M}_{lm}^{(1)}(k\mathbf{r})], \tag{5a}$$

$$\mathbf{E}_{\text{scat}} = \sum_{l=1}^{\infty} \sum_{m=-l}^{l} [a_{lm} \mathbf{N}_{lm}^{(3)}(k\mathbf{r}) + b_{lm} \mathbf{M}_{lm}^{(3)}(k\mathbf{r})], \tag{5b}$$

where $k = 2\pi n_0/\lambda$ is the wavenumber, with n_0 being the refractive index of the host medium; $\mathbf{r} = (r, \theta, \phi)$ is the spherical coordinate of the nanoparticle center, l indicates the order of multipole considered ($l = 1$ corresponds to the dipole term), and m takes the value between $-l$ and l (i.e. $|m| \leq l$). The physical meaning of l is associated with the total angular

momentum, while m represents the projection of l along the z-axis. The VSH basis functions ($\mathbf{M}_{lm}^{(\sigma)}$ and $\mathbf{N}_{lm}^{(\sigma)}$) are expressed as:

$$\mathbf{M}_{lm}^{(\sigma)}(k\mathbf{r}) = \xi_{lm}\nabla \times [\hat{r} \cdot u_{lm}^{(\sigma)}(k\mathbf{r})], \tag{6a}$$

$$\mathbf{N}_{lm}^{(\sigma)}(k\mathbf{r}) = \frac{1}{k}\nabla \times \mathbf{M}_{lm}^{(\sigma)}(k\mathbf{r}), \tag{6b}$$

where $u_{lm}^{(\sigma)}$ satisfies the scalar Helmholtz equation:

$$u_{lm}^{(\sigma)}(k\mathbf{r}) = z_{lm}^{(\sigma)}(kr)P_l^m(\cos(\theta))e^{im\phi}, \tag{7}$$

with $z_{lm}^{(\sigma)}(kr)$ for the radial part of the scalar spherical harmonics and $P_l^m(\cos(\theta))$ for the associated Legendre polynomial. The superscript (σ) assigns the type of Bessel function for $z_{lm}^{(\sigma)}$: $(\sigma) = (1)$ stands for spherical Bessel function, while $(\sigma) = (3)$ is the spherical Hankel function. The normalization of VSH in Eq. 6a (ξ_{lm}) is:

$$\xi_{lm} = \sqrt{\frac{2l+1}{4\ l(l+1)}\frac{(l-m)!}{(l+m)!}}. \tag{8}$$

In this work, the incident field is generated by a point dipole source (the donor molecule), which is modeled by replacing the typical plane wave coefficients (p_{lm}, q_{lm} in Eq. 5a) with the point dipole coefficients:[52,57,58]

$$p_{lm} = (-1)^m \left(\frac{ik^3}{n_0^2}\right) \mathbf{N}_{l(-m)}^{(3)}(k\mathbf{r}_0) \cdot \mathbf{p}, \tag{9a}$$

$$q_{lm} = (-1)^m \left(\frac{ik^3}{n_0^2}\right) \mathbf{M}_{l(-m)}^{(3)}(k\mathbf{r}_0) \cdot \mathbf{p}. \tag{9b}$$

where $\mathbf{r}_0$ is the location of the dipole (donor). Using these coefficients and the normal Mie coefficients (α_{lm}, β_{lm}), one can obtain the scattered wave coefficients (a_{lm}, b_{lm} in Eq. 5b) with the relations $a_{lm} = \alpha_{lm}p_{lm}$ and $b_{lm} = \beta_{lm}q_{lm}$.[59] Once the incident and scattered fields are determined, the total field $\mathbf{E}^{\mathrm{D}}$ in Eq. 3 can be evaluated by taking the sum of $\mathbf{E}_{\mathrm{inc}}$ and $\mathbf{E}_{\mathrm{scat}}$.

Simulation details

The simulated system in this work is a donor-acceptor pair on the opposite sides of a solid spherical silver nanoparticle (see Fig. 1). Each molecule is 10 nm from the nanoparticle surface, with a transition dipole moment pointing towards the center of the nanoparticle. Because we focus on the CF, F, the magnitudes of dipole moments have no impact on the results. The silver nanoparticle has diameters ranging from 10 nm to 230 nm. The experimental results from the work of Johnson and Christy[60] (see Supporting Information Fig. S2) is chosen to be the dielectric function of silver, smoothed by a parabolic fitting function to fill the space between experimental data points. The use of a complex dielectric function for silver ensures the inclusion of the excitonic energy absorption by the nanoparticle in our evaluation of the donor electric field, and in turns, the CF. We note that for the sizes of nanoparticles > 20 nm, the dielectric function based on Johnson and Christy provides a good description of the optical properties of silver.[61,62] On the other hand, for particles < 20 nm, the most pronounced effect on plasmon resonance lineshape due to the change in dielectric function is broadening that varies with inverse size, while the shifting of the plasmon resonance is not significantly affected.[63,64] Because the focus of this study lies more on the spectral position of the CF peaks and dips, rather than their widths, we extend the application of the Johnson and Christy dielectric function to the sizes of nanoparticles < 20 nm.

Mie theory is used to evaluate the electric field generated by the donor and the scattered field from the nanoparticle, due to its efficiency in solving electrodynamic problems for spherical nanoparticles and its expression in terms of multipoles. A total of 70 VSHs is used to ensure convergence of the calculations. Previous studies[25,26] used the finite-difference time domain (FDTD) method for the electrodynamics simulations because of its ability to solve problems for complex dielectric environments. Both methods provide fully retarded electrodynamics solutions. In the Supporting Information (SI Fig. S3), we compare the CF calculated from electric fields evaluated by both methods and show that the final results are

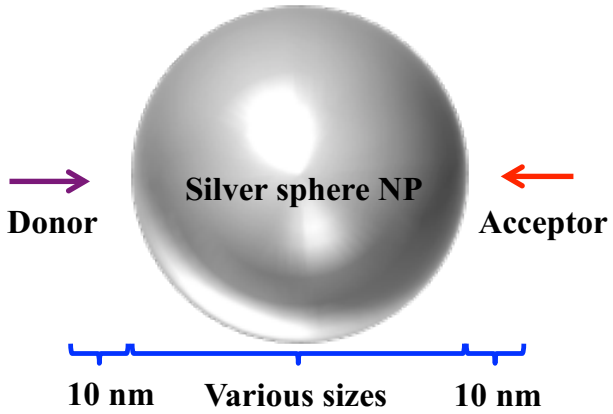

Figure 1: The simulated system. Two molecules, a donor and an acceptor, are placed on the opposite sides of a nanoparticle, with a distance of 10 nm from the molecule to the particle surface. The nanoparticle is a solid silver sphere with various diameters ranging from 15 nm to 210 nm. The transition dipoles for both the donor and the acceptor are oriented towards the center of the nanoparticle.

in agreement.

Results and Discussion

Size independence of CF

It is well-known that the peak wavelength of the extinction spectrum of a metal nanoparticle varies with its size. Fig. 2(a) shows the expected behavior of the extinction spectra for spherical silver nanoparticles, based on Mie theory with dielectric function parameters provided by Johnson and Christy.[60] For small nanoparticles, there is only one peak in the extinction spectra, such for the 30 nm and 60 nm diameter spheres (purple and blue lines), due to the dipole resonance of the particle. As the size of the nanoparticle increases, the dipole peak redshifts and broadens, while a second peak appears on the blue side. This quadrupole resonance peak is clearly distinguished for the 120 nm (brown line), 150 nm (green), and 180 nm (orange) spheres. For the largest particle shown here, the 210 nm sphere (red line), there are three peaks, including the dipole (approximately 600 nm), the quadrupole (395 nm), and the

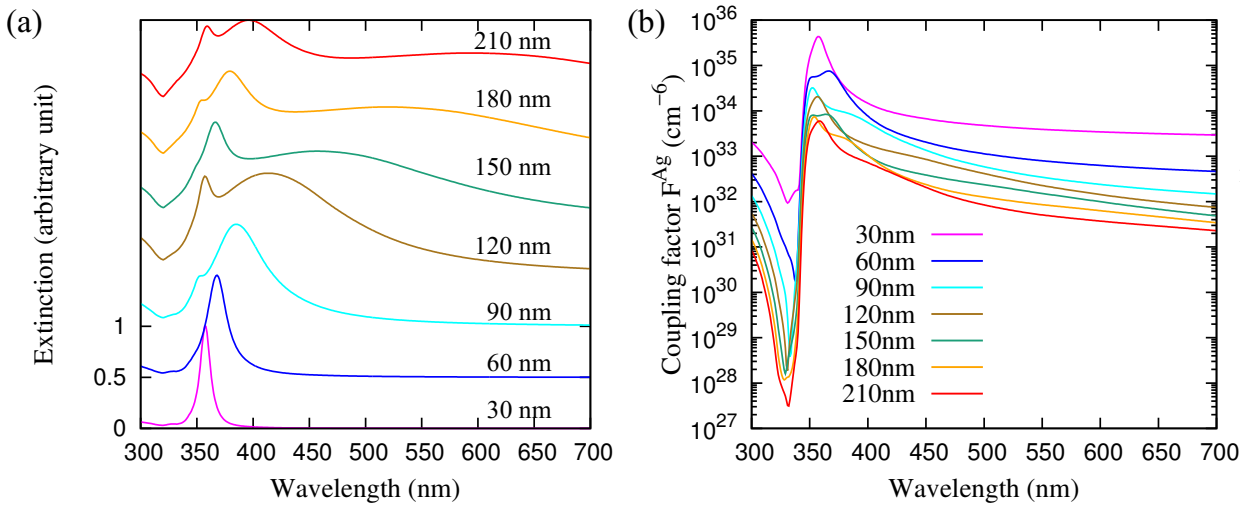

Figure 2: (a) Normalized extinction spectra of spherical silver nanoparticles with various sizes. (b) CF spectra of PC-RET in the presence of nanoparticles with various sizes.

octupole (355 nm) resonances.

It is reasonable to expect the CF spectra to exhibit behavior similar to the extinction spectra, because the two spectra are related to the scattered field from the nanoparticle. However, the aforementioned size dependence is not observed in the CF spectra shown in Fig. 2(b), and the CF spectra do not resemble the extinction efficiency spectra. First, the numbers of distinguishable peaks are different in the two types of spectra for most cases. For example, there are two peaks with similar magnitude in the CF spectrum for 60 nm particle (at $\lambda = 350$ nm and 365 nm), while only one can be seen in the extinction spectrum (365 nm). On the other hand, the 210 nm particle has one significant peak (355 nm) and one very broad but low intensity peak (395 nm) in the CF spectrum, while in the extinction spectrum, a total of 3 distinct peaks (355 nm, 395 nm, and 600 nm) are visible. Second, the relative intensity of the peaks follow different trends. For the extinction spectrum, when a nanoparticle becomes large enough to support a new, higher order multipole resonance, the corresponding peak of that resonance usually has a lower intensity compared to other peaks in the spectrum that belong to lower order multipoles. As the size of the particle increases, the intensity of this new peak grows and reaches a maximum before broadening and decaying.

This process repeats for the next higher order multipole resonance. However, this behavior is not observed in the CF spectra. Instead, a strong peak remains around 355 nm regardless of the size of the nanoparticle, while weaker peaks appear at seemingly random positions in the spectra. In later subsections, we will show that the peaks and dips in the CF spectra are related to the LSP resonance multipoles and the silver dielectric characteristics at the bulk plasmon resonance wavelength.

Origin of CF peaks for small particles: quasi-static limit

The enhancement or suppression of the CF, for the configuration in Fig. 1, is directly determined by the interference pattern of the total electric field experienced by the acceptor in the frequency domain. For small particles (< 60 nm), the total field at the position of the acceptor can be evaluated in the quasi-static limit, leading to the expression (see SI for derivation):

$$\mathbf{E}^{total}_{quasi}(\mathbf{r_A}) = \mathbf{E}^{\mathrm{D,vac}}_{quasi}(\mathbf{r_A}) \times \gamma \tag{10a}$$

$$= \frac{2\mu^{\mathrm{D}}}{R^3_{DA}} \left(1 + \frac{128 g_d a^3}{R^3_{DA}}\right) \hat{\mathbf{x}} \tag{10b}$$

where R_{DA} is the distance between the donor and the acceptor, a is the radius of the nanoparticle, and g_d is the g-factor related to the sphere dipole polarizability ($\alpha = g_d a^3$) as given by:[65]

$$g_d = \frac{\epsilon_{Ag} - 1}{\epsilon_{Ag} + 2}. \tag{11}$$

with the wavelength-dependent complex dielectric function of silver $\epsilon_{Ag}(\lambda) = \epsilon'_{Ag}(\lambda) + i\epsilon''_{Ag}(\lambda)$. Eq. 10 indicates that the total electric field is the product of the dipole field in vacuum at that position ($\mathbf{E}^{\mathrm{D,vac}}_{quasi}(\mathbf{r_A}) = 2\mu^{\mathrm{D}}/R^3_{DA}\hat{\mathbf{x}}$) and a unitless quasi-static response factor ($\gamma = 1 + 128 g_d a^3/R^3_{DA}$). This response factor γ is a quantitative measure of the interference

pattern in the frequency domain between the donor field and the nanoparticle scattered field at the position of $\mathbf{r_A}$, and includes constructive interference for $|\gamma| > 1$, and destructive interference for $|\gamma| < 1$. In addition, for this specific configuration, the CF is proportional to the absolute square of γ (i.e. $F \propto |\gamma|^2$).

The condition for any extremum of the function $|\gamma|^2$ can be obtained by taking the partial derivative of $|\gamma|^2$ with respect to ϵ'_{Ag} ($\partial|\gamma|^2/\partial\epsilon'_{Ag}$). The maximum and the minimum of the CF spectrum are found at these two points,

$$\epsilon'_{Ag} = -2 + \frac{192 \pm \sqrt{36864 + [(128 + (R_{DA}/a)^3)\epsilon''_{Ag}]^2}}{128 + (R_{DA}/a)^3}, \tag{12}$$

where the minus and plus signs correspond to the maximum and minimum, respectively. Clearly, the maximum and the minimum depend on the imaginary part of the silver dielectric function (ϵ''_{Ag}) and the ratio of the donor-acceptor distance (R_{DA}) to the radius of the particle (a). In this work, the donor-acceptor distance is always at least twice as large as the particle radius (i.e. $R_{DA}/a > 2$), regardless the particle size. For silver, ϵ''_{Ag} stays relatively constant near 0.35 between 320 nm and 700 nm. These parameters provide the maximum at $\epsilon'_{NP} \approx -2$ (i.e. around $\lambda = 355$ nm), similar to that of the extinction efficiency. On the other hand, the minimum of $|\gamma|^2$ is found between 320 nm and 340 nm, due to destructive interference in this region, which will be discussed in a later section.

The origin of the peaks in the CF spectra for small particles can be understood via the quasi-static expression for the electric field. Fig. 3 presents the comparison between the CFs calculated using the electric fields either from the quasi-static expression (Eq. 10) or from Mie theory (Eq. 5). As shown in Fig. 3(a) and (b), the CF spectra produced by the two methods qualitatively agree with each other for the cases where the nanoparticle diameters are 15 nm and 30 nm. This agreement indicates that the CF peaks for these two spheres originate from the dipole mode of the LSP resonance.

On the other hand, the quasi-static limit (Eq. 10) cannot recover the CF spectra when the

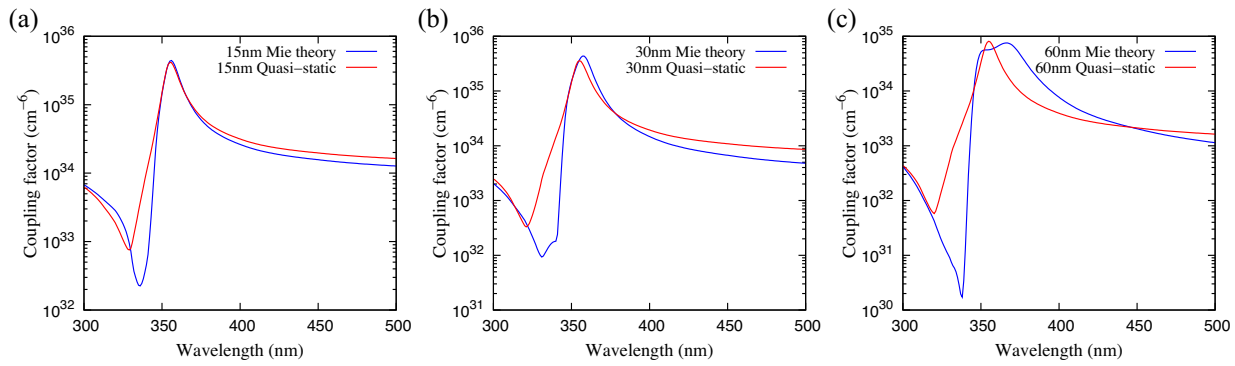

Figure 3: Comparison between CF spectra using electric field from Mie theory (blue lines) and the quasi-static method (red lines), for 15 nm (a), 30 nm (b), and 60 nm cases (c).

particle size becomes large, because the distances among the involved molecules and particles exceed the near-zone limit. The large size of the particle also introduces radiative damping and dynamic depolarization terms into the sphere dipole polarizability, which broadens and redshifts the dipole resonance peak.[65–67] The small discrepancy in peak locations for the 30 nm case (Fig. 3(b)) can be attributed to these radiative effects. Furthermore, Eq. 10 includes only the dipole resonance of the nanoparticle, while larger particles can support higher order multipoles. Hence, for the 60 nm case (Fig. 3(c)), there is only one peak from the quasi-static result, while two peaks are visible from Mie theory. The conclusions drawn from this comparison remain unchanged as long as the same dielectric function is used in both methods (see SI Fig. S4 for results using the Palik dielectric function of silver[68]).

Origin of CF peaks for large particles: LSP multipoles

To discover the origin of peaks in the CF spectra for large particles, we performed a VSH decomposition analysis on the CF spectra, which reveals the connection between the CF peaks with the LSP multipole resonances. Mie theory electric field solutions, related to the CF spectra, are constructed as a superposition of VSH basis functions with different coefficients. Therefore, one can identify the contribution of each LSP multipole resonance to the CF spectra.

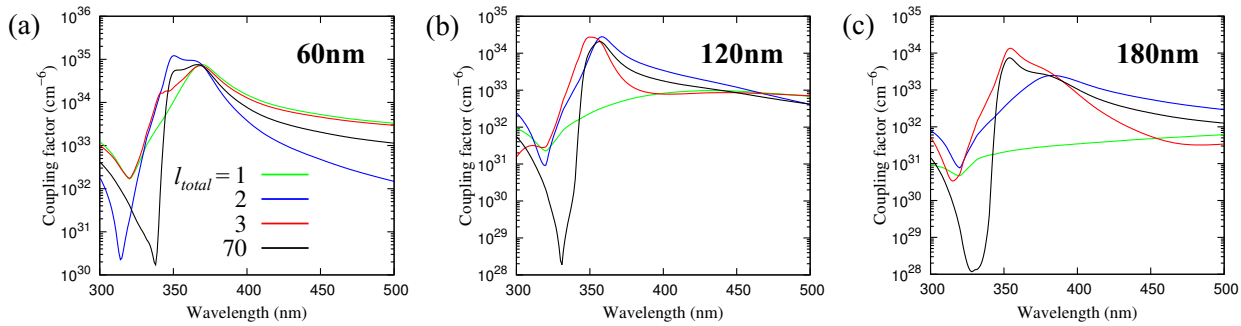

Figure 4: VSH decomposition of CF spectra for nanoparticles with sizes of 60 nm (a), 120 nm (b), and 180 nm (c). Line color labels indicate l_{total}, which is the total number of VSHs used for calculations, e.g. $l_{total} = 1$ includes only the dipole mode contribution, while $l_{total} = 2$ includes both dipole and quadrupole contributions. The converged results of CF are provided by using l_{total}=70.

Fig. 4 shows the CF spectra for nanoparticles with different sizes (60 nm, 120 nm, and 180 nm) calculated using different numbers of VSH (l_{totat}). Although calculations using a small l_{totat} are not converged, they reveal the contribution of each multipole and the cumulative effects with one VSH basis function increment. We compare the first three multipole orders: dipole, quadrupole, and octupole ($l_{totat} = 1, 2, 3$, respectively), and the converged solution ($l_{totat} = 70$). For the 60 nm case, the green line ($l_{totat} = 1$) indicates that the peak at 365 nm corresponds to the dipole resonance. When including both the dipole and the quadrupole terms (blue line), a second peak becomes visible, suggesting that the peak at 350 nm comes from the quadrupole LSP resonance. The number of peaks does not change upon the addition of the octupole resonance (red line), although the superposition modifies the magnitudes of the peaks slightly. The converged result (black line) retains two peaks in the spectrum.

Similarly, for the 120 nm and the 180 nm nanoparticles (Fig. 4 (b) and (c)), each peak in the CF spectra can be associated with a specific LSP multipole resonance. The single peak observed for the 120 nm particle is primarily from the quadrupole resonance. The octupole resonance also contributes to the intensity of the peak, but it is hard to resolve the two resonances because of their proximity to each other in wavelength. On the other hand, the

higher energy peak of the two for the 180 nm case ($\lambda = 350$ nm) is due to the octupole resonance, while the quadrupole peak is redshifted to $\lambda = 380$ nm. For both sizes, the contribution from the dipole resonance is not visible from the CF spectrum. The multipole contributions for the peaks are confirmed by visualizing the spatial map of the electric field intensity generated by FDTD (see SI Fig. S5). The VSH decompositions for other sizes are presented in the SI Fig. S6.

In order to find the correlation between the particle size and the most dominant multipole in the CF spectra, we study the change in the enhancement of the CF as the nanoparticle size increases. Here, we define a plasmon enhancement factor (Γ), which is the ratio of the CF at a certain wavelength in the presence of the nanoparticle to that in vacuum:

$$\Gamma(\lambda) = \frac{F^{\mathrm{Ag}}(\lambda)}{F^{\mathrm{Vac}}(\lambda)} \tag{13}$$

where F is defined as in Eq. 4 with the appropriate units. Fig. 5(a) presents the values of Γ at the wavelength $\lambda = 355$ nm when the particle size (diameter) changes from 10 nm to 230 nm. We choose $\lambda = 355$ nm for this analysis because Fig. 2(b) shows that the most dominant CF peak for each case is close to this wavelength. The plot shows regular oscillation in Γ as the particle size increases, giving rise to three peaks at sizes 40 nm, 120 nm, and 200 nm. These peaks can be attributed to the dipole, quadrupole, and octupole LSP resonances, respectively, as confirmed by the spatial electric field intensity maps in Fig. 5(b) - (d). The field map of the 40 nm particle shows two enhanced regions along the x-axis, separated by a node at $x = 0$, corresponding to the dipole resonance. Similarly, the four and six enhanced regions surrounding the nanoparticles in Fig. 5(c) and (d), respectively, indicates that the dominant multipole for the 120 nm particle is quadrupole, while octopole determines the CF spectra for the 200 nm particle.

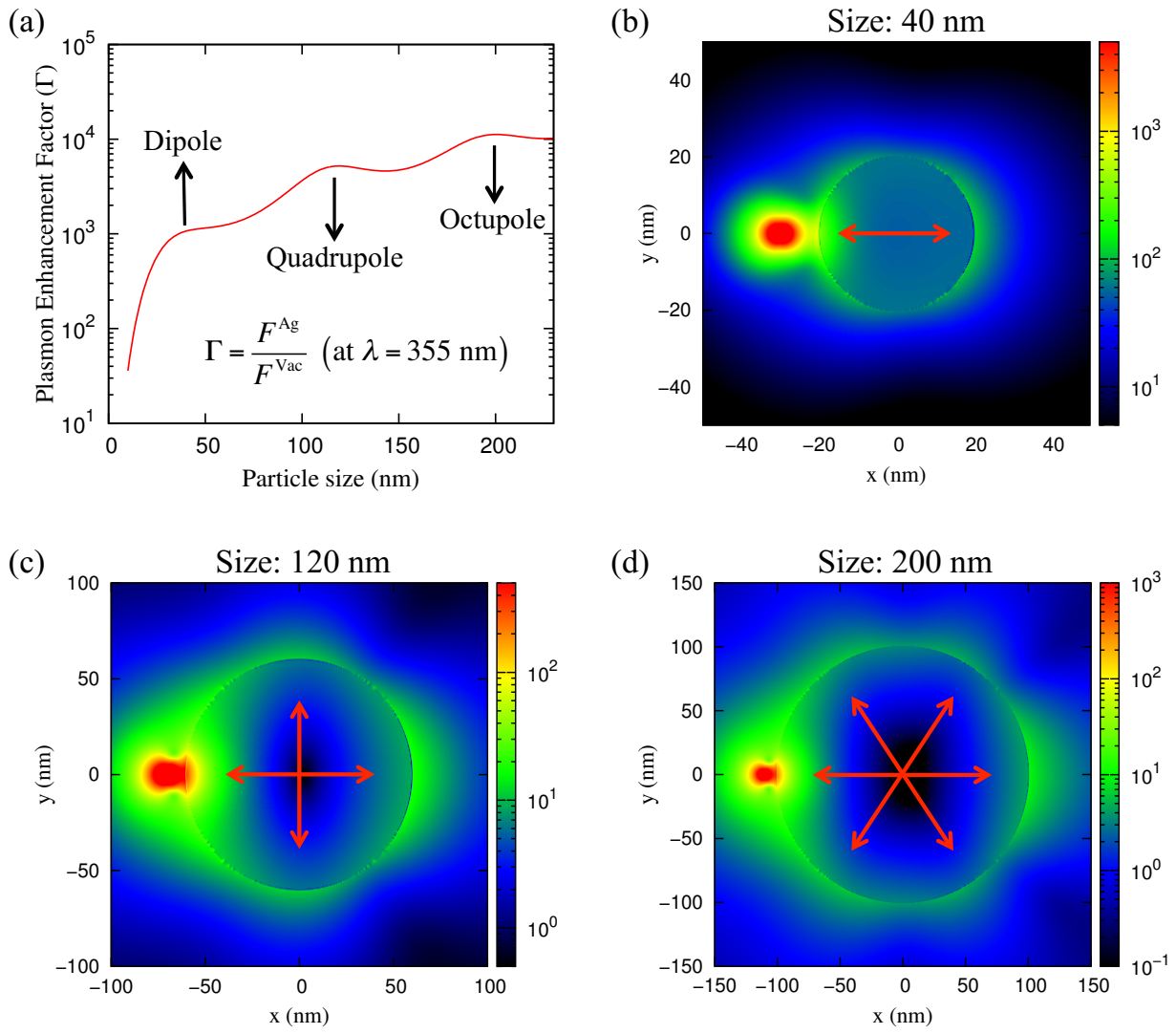

Figure 5: (a) The correlation between particle size (diameter) and plasmon enhancement factor at wavelength $\lambda = 355\,\text{nm}$. The peaks correspond to LSP multipoles. (b) - (d) The spatial electric field intensity at $\lambda = 355\,\text{nm}$ for silver nanoparticles with different sizes: 40 nm, 120 nm, and 200 nm.

Disappearance of dipole or quadrupole CF peaks for large particles

One of the main differences between the CF spectra and extinction spectra for large nanoparticles ($>$ 90 nm) is the monotonic decrease of the CF peak as wavelength increases above 400 nm, with none of the expected plasmonic multipole peaks apparent in the results in Fig. 4 This is in contrast to the appearance of peaks in the extinction spectrum in the wavelength region above 400 nm mainly due to plasmon excitation that enhances scattering from the nanoparticle.

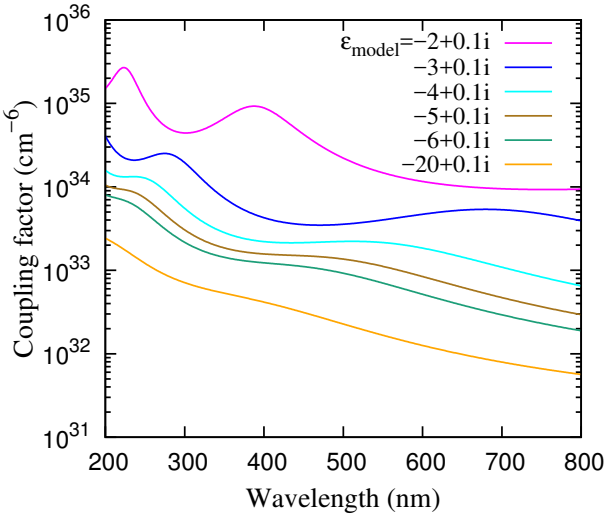

Figure 6: CF spectra for 120 nm nanoparticles with different dielectric constants: $\epsilon_{model} = \epsilon'_{model}+0.1i$, where ϵ'_{model} varies from -2 to -20. These values correspond to the silver dielectric function values in the wavelength range between 355 nm and 600 nm.

In order to illustrate the effect of dielectric function on CF spectra, we study a model system consisting of 120 nm nanoparticles with various frequency-independent dielectric constants ($\epsilon_{model} = \epsilon'_{model} + i\epsilon''_{model}$). This is to be contrasted with the silver dielectric function, which decays nearly linearly from -2 to -20 as the wavelength increases from 355 nm to 660 nm, while the imaginary part stays roughly constant at 0.35 in this region (see SI Fig. S2).[60] In the model, the nanoparticles are provided with a real part of the dielectric function ranging from -2 to -20 (i.e. $\epsilon'_{model} \in [-20, -2]$), accompanied by a small imaginary part ($\epsilon''_{model} = 0.1$). Fig. 6 shows that distinguishable CF peaks can be observed for the

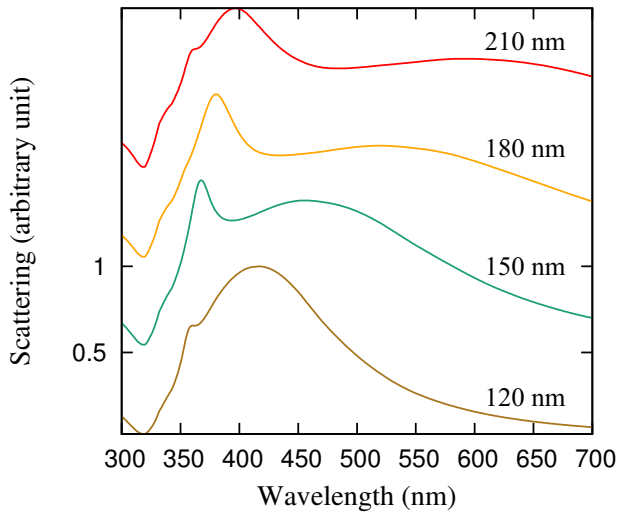

Figure 7: Normalized scattering spectra of silver spherical nanoparticles with various sizes (diameter).

model results, especially when the negative real part of the model dielectric constant is small ($\epsilon_{model} = -2 + 0.1i$). As the negative real part of ϵ_{model} becomes more negative, the model nanoparticle becomes a better absorber and plasmon modes are suppressed, causing the CF peaks to be less and less obvious. For $\epsilon_{model} = -20 + 0.1i$, the CF spectrum is mostly a straight line. Based on the numerical illustration above, we conclude that the characteristics of the silver dielectric function (the decreasing negative real part) results in the disappearance of the CF peaks at long wavelength.

On the other hand, the visible extinction peaks in the region above 400 nm are mainly due to the scattering of incident light. The extinction spectrum is the sum of the absorption and the scattering spectra.[65] Fig. 7 presents the scattering spectra of silver nanoparticles with different sizes, which shows that for large particles, scattering generates the peaks above $\lambda = 400$ nm. Note that scattered light hardly reaches the opposite side of a large nanoparticle from the donor, as the acceptor is located in a shadow region on that side of the nanoparticle. Hence, scattering does not contribute to the CF spectrum in our setup.

Origin of CF dips

The quasi-static expression, Eq. 10, can be used to explain the origin of the dips in CF spectra for small particles ($< 60\,\text{nm}$), which comes from destructive interference between the donor dipole field and the induced dipole field, influenced by the silver dielectric function. The minimum of $|\gamma|^2$ corresponds to a dip in the small particle CF spectra (selecting the plus sign in Eq. 12). Depending on the size of the nanoparticle, it is possible to find a minimum in the range of $-0.5 < \epsilon'_{Ag} < 0.85$ (i.e. $320\text{nm} < \lambda < 355\text{nm}$) for the real part of the dielectric function. For example, the minimum in $|\gamma|^2$ occurs at $\epsilon'_{Ag} = -0.26$ for 15 nm nanoparticle ($\lambda = 327\,\text{nm}$), and at $\epsilon'_{Ag} = 0.38$ for 30 nm nanoparticle ($\lambda = 321\,\text{nm}$). Again, $|\gamma|^2$ less than 1 represents destructive interference of the electric field and results in suppression of energy transfer compared to energy transfer without the nanoparticle.

For particles with 60 nm diameter or larger, we find that the CF dips are associated with a silver dielectric function $\epsilon'_{Ag} = 0$ corresponding to bulk plasmon resonance. The CF is related to the total electric field at the position of the acceptor, mediated by either propagation of the surface plasmon on the particle surface or direct penetration of the field through the nanoparticle. Around the bulk plasmon resonance wavelength of silver (325 nm), the real part of its dielectric function is zero, which does not fulfill the condition for surface plasmon excitation (which dominates at longer wavelengths).[69] Hence, the electric field emitted by the donor cannot propagate to the acceptor via the particle surface. In addition, the extinction coefficient ($\kappa_{Ag} = 0.56$) at this wavelength in combination with the large particle size prevents direct transmission through the particle to the acceptor. Therefore, the electric field at the acceptor position is very small, leading to the pronounced CF dip at this wavelength. To support our argument, spatial electric field maps for the 210 nm nanoparticle at three different wavelengths ($\lambda = 300\,\text{nm}$, 325 nm, and 355 nm) are shown in Fig. 8. Clearly, the acceptor position (red cross in plot, at $x = 115$ and $y = 0$) and its nearby region have a much weaker field at $\lambda = 325\,\text{nm}$ (CF dip), as compared to that at 300 nm or at 355 nm (CF peak). This confirms that suppression in the CF spectra is due to the lack of surface plasmon

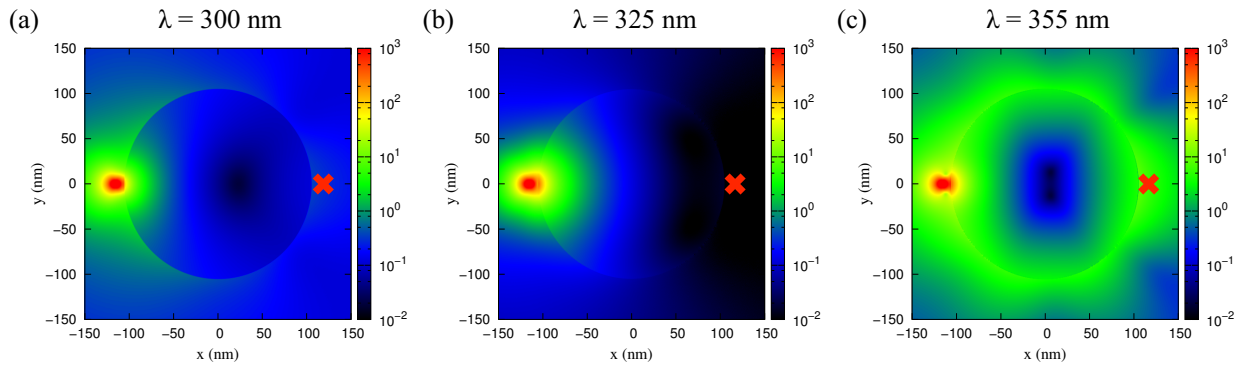

Figure 8: Electric field intensity for the 210 nm silver nanoparticle at different wavelengths: 300 nm, 325 nm, and 355 nm. The CF dip for this particle is at $\lambda = 325$ nm, while the CF peak is at $\lambda = 355$ nm. The red crosses mark the position of the acceptor in each case.

propagation. There are no plasmons at 300 nm, as the real part of the dielectric function is positive at that wavelength, however this also means that there is less damping than at 325 nm, and more direct penetration through the particle. This can be seen in Fig. 8. The CF dips and the disappearance of CF peaks indicate strong suppression of energy transfer in certain directions or frequency bands. This may be important in device applications, such as in the control of energy flow in suppressing the radiative decay of excited species.

Conclusions

The effect of a nearby nanoparticle on the resonance energy transfer between a donor and an acceptor can be understood by examining spectra associated with the electromagnetic coupling factor that appears in the energy transfer matrix element. For two molecules placed on the opposite sides of a spherical silver nanoparticle, the CF shows a peak near 355 nm and a dip near 325 nm that is surprisingly independent of nanoparticle size, and not closely related to the extinction spectrum of the nanoparticle. We have analyzed this behavior of the CF, both in the quasi-static limit for small particles, and in a fully retarded treatment for large particles, and we find that the peak near 355 nm arises from excitation of the highest order LSP multipole resonance that can be excited for a given nanoparticle size.

For small particles where the quasi-static limit applies, this enhancement can be attributed to the constructive interference between the donor dipole electric field and the scattered field from dipole LSP excitation in the nanoparticle. For larger particles, the highest LSP multipole most effectively propagates plasmon excitation around the nanoparticle. To the red of 355 nm, the CF is diminished by the large negative value of the Silver dielectric function, as this dampens field propagation through the nanoparticle, creating a shadow where the acceptor is located. Near 325 nm, surface plasmons can no longer be excited, which diminishes propagation of the excitation around the particle, leading to a minimum in the CF. For small nanoparticles, we also find that the dips in CF spectra can be understood via the concept of destructive interference of the donor field and the nanoparticle scattered field. We hope that our study will motivate the engineering of plasmon mediated resonance energy transfer at the nanoscale.

Supporting Information Available

Derivation for quasi-static expression of the electric field due to a donor dipole at the position of the acceptor, with the response of a silver nanoparticle in between; Dielectric function of silver from experimental results of Johnson and Christy; Comparison between CF results using FDTD and Mie theory for electrodynamics simulations; Comparison between CF results using Mie theory and quasi-static expression for electrodynamics simulations, but with Palik dielectric function for silver; VSH decomposition on CF spectra for nanoparticles with different sizes; Spatial map of electric field intensity at multipole resonance wavelengths.

This material is available free of charge via the Internet at `http://pubs.acs.org/`.

Acknowledgement

This work was supported by U.S. National Science Foundation under grant number CHE-1465045. Hsu thanks Academia Sinica and the Ministry of Science and Technology of Taiwan

(MOST 106-2113-M-001-036-MY3) for the financial support. Computations for this research were supported in part the Quest high performance computing facility at Northwestern University which is jointly supported by the Office of the Provost, the Office for Research, and Northwestern University Information Technology.

References

(1) Lal, S.; Grady, N. K.; Kundu, J.; Levin, C. S.; Lassiter, J. B.; Halas, N. J. Tailoring Plasmonic Substrates for Surface Enhanced Spectroscopies. *Chem. Soc. Rev.* **2008**, *37*, 898–911.

(2) Schatz, G. C.; Young, M. A.; Van Duyne, R. P. *Surface-Enhanced Raman Scattering: Physics and Applications*; Springer Berlin Heidelberg: Berlin, Heidelberg, 2006; pp 19–45.

(3) Sharma, B.; Frontiera, R. R.; Henry, A.-I.; Ringe, E.; Van Duyne, R. P. SERS: Materials, Applications, and the Future. *Mater. Today* **2012**, *15*, 16–25.

(4) Willets, K. A.; Van Duyne, R. P. Localized Surface Plasmon Resonance Spectroscopy and Sensing. *Annu. Rev. Phys. Chem.* **2007**, *58*, 267–297.

(5) Ross, M. B.; Ashley, M. J.; Schmucker, A. L.; Singamaneni, S.; Naik, R. R.; Schatz, G. C.; Mirkin, C. A. Structure-Function Relationships for Surface-Enhanced Raman Spectroscopy-Active Plasmonic Paper. *J. Phys. Chem. C* **2016**, *120*, 20789–20797.

(6) Oulton, R. F.; Sorger, V. J.; Zentgraf, T.; Ma, R.-M.; Gladden, C.; Dai, L. D.; Bartal, G.; Zhang, X. Plasmon Lasers at Deep Subwavelength Scale. *Nature* **2009**, *461*, 629–632.

(7) Zhou, W.; Odom, T. W. Tunable Subradiant Lattice Plasmons by Out-of-Plane Dipolar Interactions. *Nat. Nanotech.* **2011**, *6*, 423–427.

(8) Zhou, W.; Dridi, M.; Suh, J. Y.; Kim, C. H.; Co, D. T.; Wasielewski, M. R.; Schatz, G. C.; Odom, T. W. Lasing Action in Strongly Coupled Plasmonic Nanocavity Arrays. *Nat. Nanotech.* **2013**, *8*, 506–511.

(9) Yun, C. S.; Javier, A.; Jennings, T.; Fisher, M.; Hira, S.; Peterson, S.; Hopkins, B.; Reich, N. O.; Strouse, G. F. Nanometal Surface Energy Transfer in Optical Rulers, Breaking the FRET Barrier. *J. Am. Chem. Soc.* **2005**, *127*, 3115–3119.

(10) Mayer, K. M.; Hafner, J. H. Localized Surface Plasmon Resonance Sensors. *Chem. Rev.* **2011**, *111*, 3828–3857.

(11) Saha, K.; Agasti, S. S.; Kim, C.; Li, X.; Rotello, V. M. Gold Nanoparticles in Chemical and Biological Sensing. *Chem. Rev.* **2012**, *112*, 2739–2779.

(12) Li, M.; Cushing, S. K.; Wu, N. Plasmon-Enhanced Optical Sensors: A Review. *Analyst* **2015**, *140*, 386–406.

(13) Kong, X.-T.; Khosravi Khorashad, L.; Wang, Z.; Govorov, A. O. Photothermal Circular Dichroism Induced by Plasmon Resonances in Chiral Metamaterial Absorbers and Bolometers. *Nano Lett.* **2018**, *18*, 2001–2008, PMID: 29420903.

(14) Yu, B.; Tracey, J. I.; Cheng, Z.; Vacha, M.; O'Carroll, D. M. Plasmonic Sphere-on-Plane Systems with Semiconducting Polymer Spacer Layers. *Phys. Chem. Chem. Phys.* **2018**, *20*, 11749–11757.

(15) Catchpole, K.; Polman, A. Plasmonic Solar Cells. *Opt. Express* **2008**, *16*, 21793–21800.

(16) Pillai, S.; Catchpole, K. R.; Trupke, T.; Green, M. A. Surface Plasmon Enhanced Silicon Solar Cells. *J. Appl. Phys.* **2007**, *101*, 093105.

(17) Nakayama, K.; Tanabe, K.; Atwater, H. A. Plasmonic Nanoparticle Enhanced Light Absorption in GaAs Solar Cells. *Appl. Phys. Lett.* **2008**, *93*, 121904.

(18) Bujak, Ł.; Narushima, K.; Sharma, D. K.; Hirata, S.; Vacha, M. Plasmon Enhancement of Triplet Exciton Diffusion Revealed by Nanoscale Imaging of Photochemical Fluorescence Upconversion. *J. Phys. Chem. C* **2017**, *121*, 25479–25486.

(19) Narushima, K.; Hirata, S.; Vacha, M. Nanoscale Sriplet Exciton Diffusion via Imaging of Up-conversion Emission from Single Hybrid Nanoparticles in Molecular Crystals. *Nanoscale* **2017**, *9*, 10653–10661.

(20) Yu, P.; Zhang, F.; Li, Z.; Zhong, Z.; Govorov, A.; Fu, L.; Tan, H.; Jagadish, C.; Wang, Z. Giant Optical Pathlength Enhancement in Plasmonic Thin Film Solar Cells Using Core-Shell Nanoparticles. *J. Phys. D* **2018**, *51*, 295106.

(21) Bidault, S.; Devilez, A.; Ghenuche, P.; Stout, B.; Bonod, N.; Wenger, J. Competition between Förster Resonance Energy Transfer and Donor Photodynamics in Plasmonic Dimer Nanoantennas. *ACS Photon.* **2016**, *3*, 895–903.

(22) de Torres, J.; Mivelle, M.; Moparthi, S. B.; Rigneault, H.; Van Hulst, N. F.; García-Parajó, M. F.; Margeat, E.; Wenger, J. Plasmonic Nanoantennas Enable Forbidden F orster Dipole-Dipole Energy Transfer and Enhance the FRET Efficiency. *Nano Lett.* **2016**, *16*, 6222–6230.

(23) Poudel, A.; Chen, X.; Ratner, M. A. Enhancement of Resonant Energy Transfer Due to an Evanescent Wave from the Metal. *J. Phys. Chem. Lett.* **2016**, *7*, 955–960.

(24) Poudel, A.; Chen, X.; Ratner, M. A. Resonant Energy Transfer under the Influence of the Evanescent Field from the Metal. *J. Chem. Phys.* **2017**, *146*, 244115.

(25) Ding, W.; Hsu, L.-Y.; Schatz, G. C. Plasmon-Coupled Resonance Energy Transfer: A Real-Time Electrodynamics Approach. *J. Chem. Phys.* **2017**, *146*, 064109.

(26) Hsu, L.-Y.; Ding, W.; Schatz, G. C. Plasmon-Coupled Resonance Energy Transfer. *J. Phys. Chem. Lett.* **2017**, *8*, 2357–2367.

(27) Bujak, Ł.; Ishii, T.; Sharma, D. K.; Hirata, S.; Vacha, M. Selective Turn-On and Modulation of Resonant Energy Transfer in Single Plasmonic Hybrid Nanostructures. *Nanoscale* **2017**, *9*, 1511–1519.

(28) Sundström, V.; Pullerits, T.; van Grondelle, R. Photosynthetic Light-Harvesting: Reconciling Dynamics and Structure of Purple Bacterial LH2 Reveals Function of Photosynthetic Unit. *J. Phys. Chem. B* **1999**, *103*, 2327–2346.

(29) Scholes, G. D.; Fleming, G. R. On the Mechanism of Light Harvesting in Photosynthetic Purple Bacteria: B800 to B850 Energy Transfer. *J. Phys. Chem. B* **2000**, *104*, 1854–1868.

(30) Mohseni, M.; Rebentrost, P.; Lloyd, S.; Aspuru-Guzik, A. Environment-Assisted Quantum Walks in Photosynthetic Energy Transfer. *J. Chem. Phys.* **2008**, *129*, 174106.

(31) Beljonne, D.; Curutchet, C.; Scholes, G. D.; Silbey, R. J. Beyond Förster Resonance Energy Transfer in Biological and Nanoscale Systems. *J. Phys. Chem. B* **2009**, *113*, 6583–6599.

(32) Wu, P.; Brand, L. Resonance Energy Transfer: Methods and Applications. *Anal. Biochem.* **1994**, *218*, 1–13.

(33) Deniz, A. A.; Dahan, M.; Grunwell, J. R.; Ha, T.; Faulhaber, A. E.; Chemla, D. S.; Weiss, S.; Schultz, P. G. Single-Pair Fluorescence Resonance Energy Transfer on Freely Diffusing Molecules: Observation of Förster Distance Dependence and Subpopulations. *Proc. Natl. Acad. Sci. U.S.A.* **1999**, *96*, 3670–3675.

(34) Margittai, M.; Widengren, J.; Schweinberger, E.; Schröder, G. F.; Felekyan, S.; Haustein, E.; König, M.; Fasshauer, D.; Grubmüller, H.; Jahn, R. et al. Single-Molecule

Fluorescence Resonance Energy Transfer Reveals a Dynamic Equilibrium Between Closed and Open Conformations of Syntaxin 1. *Proc. Natl. Acad. Sci. U.S.A.* **2003**, *100*, 15516–15521.

(35) Brustad, E. M.; Lemke, E. A.; Schultz, P. G.; Deniz, A. A. A General and Efficient Method for the Site-Specific Dual-Labeling of Proteins for Single Molecule Fluorescence Resonance Energy Transfer. *J. Am. Chem. Soc.* **2008**, *130*, 17664–17665.

(36) Hanson, J. A.; Yang, H. Quantitative Evaluation of Cross Correlation Between Two Finite-Length Time Series with Applications to Single-Molecule FRET. *J. Phys. Chem. B* **2008**, *112*, 13962–13970.

(37) Yang, H. The Orientation Factor in Single-Molecule Förster-Type Resonance Energy Transfer, with Examples for Conformational Transitions in Proteins. *Isr. J. Chem.* **2009**, *49*, 313–321.

(38) Haas, K. R.; Yang, H.; Chu, J.-W. Expectation-Maximization of the Potential of Mean Force and Diffusion Coefficient in Langevin Dynamics from Single Molecule FRET Data Photon by Photon. *J. Phys. Chem. B* **2013**, *117*, 15591–15605.

(39) Dong, H.; Gao, W.; Yan, F.; Ji, H.; Ju, H. Fluorescence Resonance Energy Transfer between Quantum Dots and Graphene Oxide for Sensing Biomolecules. *Anal. Chem.* **2010**, *82*, 5511–5517.

(40) Dennis, A. M.; Rhee, W. J.; Sotto, D.; Dublin, S. N.; Bao, G. Quantum Dot-Fluorescent Protein FRET Probes for Sensing Intracellular pH. *ACS Nano* **2012**, *6*, 2917–2924.

(41) Goldman, E. R.; Medintz, I. L.; Whitley, J. L.; Hayhurst, A.; Clapp, A. R.; Uyeda, H. T.; Deschamps, J. R.; Lassman, M. E.; Mattoussi, H. A Hybrid Quantum Dot-Antibody Fragment Fluorescence Resonance Energy Transfer-Based TNT Sensor. *J. Am. Chem. Soc.* **2005**, *127*, 6744–6751.

(42) Förster, T. Zwischenmolekulare Energiewanderung und Fluoreszenz. *Ann. Phys. (Berlin)* **1948**, *437*, 55–75.

(43) Scholes, G. D. Long-Range Resonance Energy Transfer in Molecular Systems. *Annu. Rev. Phys. Chem.* **2003**, *54*, 57–87.

(44) Stryer, L.; Haugland, R. P. Energy Transfer: A Spectroscopic Ruler. *Proc. Natl. Acad. Sci. USA* **1967**, *58*, 719–726.

(45) dos Remedios, C. G.; Moens, P. D. J. Fluorescence Resonance Energy Transfer Spectroscopy Is a Reliable "Ruler" for Measuring Structural Changes in Proteins. *J. Struct. Biol.* **1995**, *115*, 175–185.

(46) Zhang, J.; Fu, Y.; Lakowicz, J. R. Enhanced Förster Resonance Energy Transfer (FRET) on a Single Metal Particle. *J. Phys. Chem. C* **2007**, *111*, 50–56.

(47) Zhang, X.; Marocico, C. A.; Lunz, M.; Gerard, V. A.; Gun'ko, Y. K.; Lesnyak, V.; Gaponik, N.; Susha, A. S.; Rogach, A. L.; Bradley, A. L. Experimental and Theoretical Investigation of the Distance Dependence of Localized Surface Plasmon Coupled Förster Resonance Energy Transfer. *ACS Nano* **2014**, *8*, 1273–1283.

(48) Power, E. A.; Thirunamachandran, T. Quantum Electrodynamics with Nonrelativistic Sources. III. Intermolecular Interactions. *Phys. Rev. A* **1983**, *28*, 2671–2675.

(49) Andrews, D. L.; Sherborne, B. S. Resonant Excitation Transfer: A Quantum Electrodynamical Study. *J. Chem. Phys.* **1987**, *86*, 4011–4017.

(50) Juzeliūnas, G.; Andrews, D. L. Quantum Electrodynamics of Resonant Energy Transfer in Condensed Matter. *Phys. Rev. B* **1994**, *49*, 8751–8763.

(51) Dung, H. T.; Knöll, L.; Welsch, D.-G. Intermolecular Energy Transfer in the Presence of Dispersing and Absorbing Media. *Phys. Rev. A* **2002**, *65*, 043813.

(52) Heaps, C. W.; Schatz, G. C. Modeling Super-Resolution SERS Using a T-matrix Method to Elucidate Molecule-Nanoparticle Coupling and the Origins of Localization Errors. *J. Chem. Phys.* **2017**, *146*, 224201.

(53) Mackowski, D. W. Analysis of Radiative Scattering for Multiple Sphere Configurations. *Proc. R. Soc. A* **1991**, *433*, 599–614.

(54) Mackowski, D. W. Calculation of Total Cross Sections of Multiple-Sphere Clusters. *J. Opt. Soc. Am. A* **1994**, *11*, 2851–2861.

(55) Mackowski, D. W.; Mishchenko, M. I. Calculation of the T Matrix and the Scattering Matrix for Ensembles of Spheres. *J. Opt. Soc. Am. A* **1996**, *13*, 2266–2278.

(56) Mackowski, D. W.; Mishchenko, M. I. A Multiple Sphere T-matrix Fortran Code for Use on Parallel Computer Clusters. *J. Quant. Spectrosc. Radiat. Transf.* **2011**, *112*, 2182–2192.

(57) Kerker, M.; Wang, D.-S.; Chew, H. Surface Enhanced Raman Scattering (SERS) by Molecules Adsorbed at Spherical Particles: Errata. *Appl. Opt.* **1980**, *19*, 4159–4174.

(58) Ausman, L. K.; Schatz, G. C. On the Importance of Incorporating Dipole Reradiation in the Modeling of Surface Enhanced Raman Scattering from Spheres. *J. Chem. Phys* **2009**, *131*, 084708.

(59) Bohren, C. F.; Huffman, D. *Absorption and Scattering of Light by Small Particles*; Wiley-VCH, 1983.

(60) Johnson, P. B.; Christy, R. W. Optical Constants of the Noble Metals. *Phys. Rev. B* **1972**, *6*, 4370–4379.

(61) McMahon, J. M.; Wang, Y.; Sherry, L. J.; Van Duyne, R. P.; Marks, L. D.; Gray, S. K.; Schatz, G. C. Correlating the Structure, Optical Spectra, and Electrodynamics of Single Silver Nanocubes. *J Phys. Chem. C* **2009**, *113*, 2731–2735.

(62) McPeak, K. M.; Jayanti, S. V.; Kress, S. J. P.; Meyer, S.; Iotti, S.; Rossinelli, A.; Norris, D. J. Plasmonic Films Can Easily Be Better: Rules and Recipes. *ACS Photonics* **2015**, *2*, 326–333.

(63) Kraus, W. A.; Schatz, G. C. Plasmon Resonance Broadening in Small Metal Particles. *J. Chem. Phys.* **1983**, *79*, 6130–6139.

(64) Kreibig, U.; Fragstein, C. v. The Limitation of Electron Mean Free Path in Small Silver Particles. *Z. Phys.* **1969**, *224*, 307–323.

(65) Kelly, K. L.; Coronado, E.; Zhao, L. L.; Schatz, G. C. The Optical Properties of Metal Nanoparticles: The Influence of Size, Shape, and Dielectric Environment. *J. Phys. Chem. B* **2003**, *107*, 668–677.

(66) Meier, M.; Wokaun, A. Enhanced Fields on Large Metal Particles: Dynamic Depolarization. *Opt. Lett.* **1983**, *8*, 581–583.

(67) Moroz, A. Depolarization Field of Spheroidal Particles. *J. Opt. Soc. Am. B* **2009**, *26*, 517–527.

(68) Palik, E. D.; Ghosh, G. *Handbook of Optical Constants of Solids*; San Diego: Academic Press., 1998.

(69) Novotny, L.; Hecht, B. *Principles of Nano-Optics*; Cambridge, 2006.

Graphical TOC Entry